Journal Pre-proofs

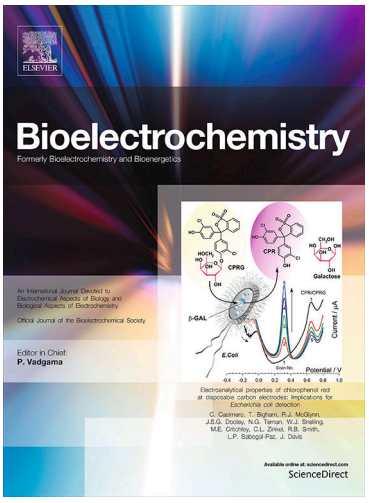

Amperometric determination of heavy metal using an HRP inhibition biosensor based on ITO nanoparticles-ruthenium (III) hexamine trichloride composite: central composite design optimization

Berna Dalkıran

PII: S1567-5394(19)30869-2
DOI: https://doi.org/10.1016/j.bioelechem.2020.107569
Reference: BIOJEC 107569

To appear in: *Bioelectrochemistry*

Received Date: 19 December 2019
Revised Date: 13 May 2020
Accepted Date: 13 May 2020

Please cite this article as: B. Dalkıran, Amperometric determination of heavy metal using an HRP inhibition biosensor based on ITO nanoparticles-ruthenium (III) hexamine trichloride composite: central composite design optimization, *Bioelectrochemistry* (2020), doi: https://doi.org/10.1016/j.bioelechem.2020.107569

Amperometric determination of heavy metal using an HRP inhibition biosensor based on ITO nanoparticles-ruthenium (III) hexamine trichloride composite: central composite design optimization

Berna Dalkıran

Ankara University, Faculty of Science, Department of Chemistry, Ankara, Turkey
Tel.: +903122126720/1293; Fax.: +903122232395
E-mail address:bernadalkiran@gmail.com

Abstract

A novel horseradish peroxidase (HRP) enzyme inhibition biosensor based on indium tin oxide (ITO) nanoparticles, hexaammineruthenium (III) chloride (RUT), and chitosan (CH) modified GCE was developed. The biosensor fabrication process was investigated using scanning electron microscopy, energy-dispersive X-ray spectroscopy, cyclic voltammetry, and electrochemical impedance spectroscopy. The amounts of ITO nanoparticles and RUT were optimized using a 2^2 central composite design for the optimization of electrode composition. The detection limits were determined as 8 nM, 3 nM, and 1 nM for Pb^{2+}, Ni^{2+}, and Cd^{2+}, respectively. The inhibition calibration curves of the biosensor were found to be within the range of 0.009–0.301 μM with a sensitivity of 11.97 $\mu A \mu M^{-1} cm^{-2}$ (0.85 $\mu A \mu M^{-1}$) for Pb^{2+}, 0.011–0.368 μM with a sensitivity of 10.84 $\mu A \mu M^{-1}\ cm^{-2}$ (0.77 $\mu A \mu M^{-1}$) for Ni^{2+}, and 0.008–0.372 μM with a sensitivity of 10.99 $\mu A \mu M^{-1} cm^{-2}$ (0.78 $\mu A \mu M^{-1}$) for Cd^{2+}. The type of HRP inhibition by Pb^{2+}, Ni^{2+} and Cd^{2+} was investigated by the Dixon and Cornish-Bowden plots. The effects of possible interfering species on the biosensor response were examined. The analysis of Pb^{2+}, Ni^{2+}, and Cd^{2+} in tap water was demonstrated using the HRP/ITO-RUT-CH/GCE with satisfactory experimental results. The proposed method agreed with the atomic absorption spectrometry results.

Keywords: enzyme inhibition; heavy metal; horseradish peroxidase; biosensor; central composite design; ITO nanoparticles

1. Introduction

Pollution from heavy metals is a critical problem that can seriously threaten the environment and human health; even trace levels of these metals are highly toxic [1]. Heavy metals can strongly interact with certain enzymes and prompt changes to the proper functioning of enzymes, thus leading to toxicological effects on living organisms [2, 3]. Therefore, a simple, rapid, and reliable method for monitoring the toxicity of drinking water and food is crucial to determine acceptable levels of heavy metals. The maximum acceptable levels of heavy metal ions in drinking water have been specified by the World Health Organization (WHO); for the sake of safety, the levelsof these metals should not exceed 0.005 mg/L of Cd^{2+}, 0.01 mg/L of Pb^{2+}, and 0.07 mg/L of Ni^{2+}, respectively [4]. Different analytical methods, such as coupled plasma flame atomic absorption spectrometry [5], atomic emission spectrometry [6], and high-performance liquid chromatography [7] have been utilized for the determination of heavy metals. However, these techniques require expensive equipment, extended periods of time, complicated laboratory processes, and highly trained analysts. On the contrary, enzyme-based biosensors have been revealed as an alternative to classical methods of monitoring trace metal ions due to their favorable properties, such as low costs, easy operation, small-sized devices, short-time analysis, high selectivity, and sensitivity [8–11]. In recent years, enzyme inhibition biosensors have been designed for the assay of heavy metals because some biosensors can act as an inhibitor of enzyme activity. [12]. In the literature, many studies on enzyme inhibition biosensors have reported the analysis of toxic metals using a degree of inhibition [12–15]. Various enzymes have been used for the detection of Cd^{2+}, Pb^{2+}, and Cu^{2+} using urease and glucose oxidase [16], Hg^{2+} using catalase [17], Hg^{2+} using urease [18], and Cd^{2+}, Pb^{2+}, and Hg^{2+} using HRP [19]. HRP was preferred for this study because it has high activity within the wide range of pH, it is commercially available in its pure form, and it has long-term stability for metal inhibition [20, 21]. This study expanded the application of inhibition biosensors for the determination of nickel with cadmium and lead and improved the limit of detection (LOD) of these metals.

Nanoparticles are mostly used for the construction of more sensitive enzyme inhibition biosensors because they offer exclusive characteristics, including the enhancement of electron transfer, good biocompatibility, catalytic efficiency, and high conductivity [22–24]. Indium tin oxide (ITO) has been widely used in electrochemical sensing because of its electrical conductivity and optoelectronic characteristics [25, 26]. In recent years, there has been a growing interest in ITO nanoparticles modified electrodes for biosensor design since they have

important physical and electrical properties such as high electrical conductivity, stability for nanometric high surface area depositions, substrate adhesion, and low capacitive current. However, only a few studies have been based on ITO nanoparticles modified electrodes [27, 28]. Like nanomaterials, artificial mediators have excellent electron transfer capabilities. They are commonly used in the development of biosensors to improve the selectivity and sensitivity of amperometric response [29, 30]. They accelerate the electron transfer between the enzyme and the surface of the electrode and enhance the improvement of electrochemical properties due to their high electrical conductivity and enhanced electrocatalysis [31–34]. They allow detection at low working potentials, thus avoiding the effect of common electrochemical interferences. Various electron transfer mediators, such as ferrocene [35], poly (neutral red) [36], and benzoquinone [37], were reported for the fabrication of enzyme inhibition biosensors. Morris et al. [38] and Ryabov et al. [39] determined that ruthenium (III) hexamine trichloride (RUT) could be used as a mediator due to its good electrocatalytic activity.

In this study, a simple and fast horseradish peroxidase (HRP) inhibition biosensor was developed to determine Pb^{2+}, Ni^{2+} and, Cd^{2+} ions in tap water with good selectivity and sensitivity. The type of inhibition was investigated using Dixon plots and Cornish-Bowden plots. For the first time, ITO nanoparticles were used in combination with RUT using chitosan (CH), a natural biopolymer that offers good film-forming ability as a dispersant [10]. The use of ITO nanoparticles and RUT together in the construction of the biosensor improved its analytical characteristics due to a synergistic catalytic effect between the ITO nanoparticles and RUT. The influence of these composites on the biosensor response was evaluated using a central composite design (CCD) as an alternative to the traditional optimization method. In the literature, there are a limited number of studies based on the combination of nanomaterials and mediators for the monitoring of heavy metals [40, 41]. Even though many enzyme biosensors have been applied to the analysis of Pb^{2+} and Cd^{2+} [14, 19, 42-44], there are fewer studies concerning the determination of Ni^{2+} [45]. In addition to lead and cadmium, nickel, which can cause health problems, such as cancer, chronic asthma, dermatitis, and allergies, was also chosen in the study due to the fact that it leaches from metals that come into contact with drinking water, such as pipes and fittings [4, 46]. To the best of the author's knowledge, an amperometric HRP inhibition biosensor has not been previously used for the detection of Ni^{2+} ion. In the current study, sensitive and selective HRP inhibition biosensors were applied to the determination of Pb^{2+}, Ni^{2+}, and Cd^{2+} in tap water. The obtained results from the proposed method agreed with the atomic absorption spectrometry (AAS) results.

2. Experimental

2.1 Reagents and solutions

Peroxidase from horseradish (HRP, E.C. 1.11.1.7, 200 units mg^{-1} solid), Nafion (5% w/w in lower aliphatic alcohols), potassium hexacyanoferrate (II) trihydrate, potassium hexacyanoferrate (III), potassium chloride, bovine serum albumin (BSA), glutaraldehyde (GA), acetic acid, and hydrogen peroxide (30% w/w in H_2O) were obtained from Sigma. The indium tin oxide (ITO) nanoparticles (<50 nm particle size), ruthenium (III) hexamine trichloride (RUT) (95%), and chitosan (CH) (medium molecular weight) were from Aldrich. Disodium hydrogen phosphate and sodium dihydrogen phosphate were from Riedel-deHaën. Lead(II), nickel(II), cadmium(II), mercury(II), manganese(II), iron(II), calcium(II), zinc(II), magnesium(II), sodium(I), and potassium(I) solutions were prepared using AAS standard solutions (1.000 g/l, Merck) and diluted with distilled water. Ethylenedinitrilotetraacetic acid was purchased from Merck and 0.1 M NaOH (Merck) was used to adjust the pH value. The pH of the tap water samples was adjusted to 6.50 with 0.10 M HCl for the application of the biosensor.

2.2 Apparatus and measurements

Electrochemical measurements were performed using an Ivium CompactStat electrochemical analyzer (Ivium Technologies, Netherlands). The electrochemical system consistedof three electrodes: Ag|AgCl reference, platinum counter, and glassy carbon electrode (GCE). All amperometric measurements were carried out at −0.25 V vs. Ag/AgCl electrodes in a phosphate buffer solution (PBS) (0.05 M, pH 6.5) under a controlled magnetic string. When the working electrode reached the steady-state, the current (i_0) was recorded. An aliquot of substrate stock solution was added to the electrochemical cell and the steady current values were recorded (i). In the amperometric measurements, the current differences ($\Delta i=i–i0$) were plotted against the substrate concentration. The pH value of the solutions was adjusted using a Thermo Orion–720A pH ion-meter and combined pH glass electrode. The morphology of the electrodes was investigated using scanning electron microscopy (SEM) (FEI, Quanta 450 FEG), and energy-dispersive X-ray spectroscopy was applied using a Bruker detector. All aqueous solutions were prepared with deionized water (ELGA PureLab Classic Ultrapure Water System). The electrochemical surface characteristics of the prepared electrodes were investigated using 0.1 M KCl solution containing 5.0 mM of the ferri/ferrocyanide redox couple with cyclic voltammetry and electrochemical impedance spectroscopy (EIS) methods. EIS studies were carried out at 0.2 V with an amplitude of 0.01 mV within a frequency range of

10^5–0.05 Hz. The sample was analyzed using atomic absorption spectrometry (GBC Avanta PM-GF 3000, Australia). All amperometric studies were performed at room temperature in phosphate buffer solution (PBS) (0.05 M).

2.3 Central composite design

A central composite design (CCD), a statistical and mathematical method, was used to study the effects of the parameters and the interaction between them. The general second-order polynomial model is given as 'Eq. (1)'[47]:

$$\hat{y} = b_0 + b_1x_1 + b_2x_2 + b_{11}x_1^2 + b_{22}x_2^2 + b_{12}x_1x_2 \quad (1)$$

where $\hat{y}$ is the predicted response for amperometric measurement, b_0, b_1, b_2, b_{11}, b_{22} and b_{12} are regression coefficients, and x_1 and x_2 represent experimental levels of the independent variables. In this work, the effect of ITO nanoparticles and RUT concentration on the response of the modified electrode were examined using the CCD model. CCD was used in the experimental design for optimization using Design-Expert® software (Version 10.0.3, Stat-Ease, Minneapolis, USA), and ANOVA analysis was applied (95% confidence level, $p = 0.05$).

2.4 Biosensor preparation

The bare GCE surface was polished before each experiment with alumina powder (0.05 μm). The polished GCE was sonicated in ethanol and distilled water. The ITO nanoparticles (5.9 mg) and RUT (3.4 mg) were dispersed into 1 mL of 5mg/mL CH solution (in pH 5.0, 100 mM acetic acid) and 7.5 μL of the dispersed solution was dropped onto the GCE surface and allowed to dry at room temperature. An HRP solution, with a concentration of 8 mg/mL, was prepared in 0.1 M PBS (pH 6.0).Subsequently, 4.0 μL HRP, 2.5 μL CH, and 0.07 mg (1%) BSA were mixed, ultrasonically, for 10 min. Then, 0.3 μL of GA (2.5%) was added to the mixture and ultrasonicated again for 10 min. A proper amount of the prepared enzyme solution was spread onto the modified electrode surface. The HRP/ITO-RUT-CH/GCE was dried in the air for approximately two hours. Finally, 5 μL of Nafion solution (1:1) was cast onto the modified enzyme electrode and dried. The preparation of the biosensor is described in Fig. 1.

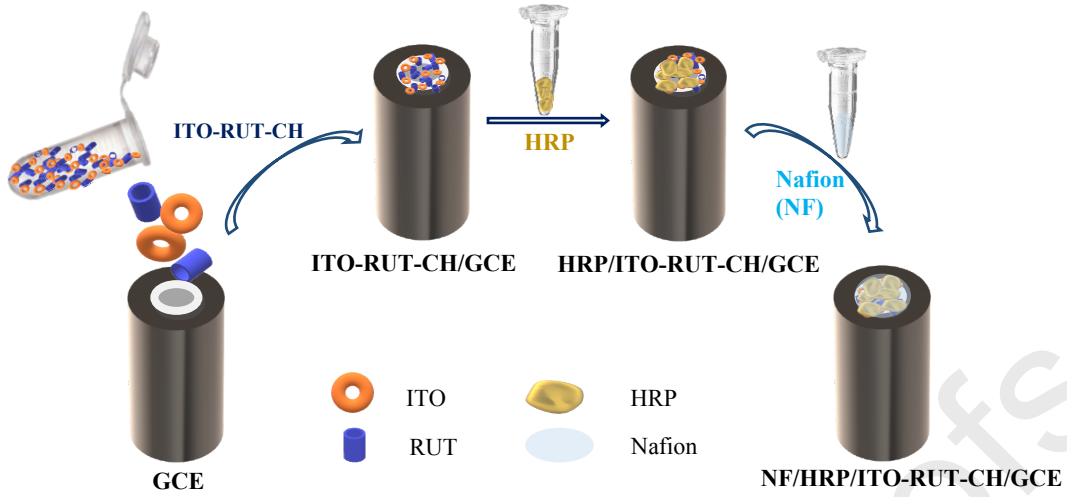

Fig. 1. The fabrication steps for the HRP/ITO-RUT-CH/GCE

2.5 Enzyme inhibition procedure

The HRP/ITO-RUT-CH/GCE was immersed into a stirred 0.05 M PBS. A known quantity of H_2O_2 was added after reaching a stable baseline current and the observed steady-state current (I_0) was recorded. After adding the inhibitor (Pb^{2+}, Ni^{2+}, Cd^{2+}) in the presence of H_2O_2, the current decreased (I_1). The increased concentration of heavy metal leads to the inhibition of enzyme activity. The reduction in the resulting current (I_1) is directly proportional to inhibitor concentration. The percent of inhibition (I %) was calculated using Eq. (2), suggested by Guascito et al. (2008) [48].

$$I(\%) = \frac{I_0 - I_1}{I_0} \times 100 \qquad (2)$$

3. Results and discussion

3.1. Surface morphological and electrochemical characterization of modified electrodes

Surface characterization studies of modified electrodes were investigated using SEM and energy-dispersive X-ray spectroscopy (EDX). The SEM images of GCEs modified with ITO-CH, RUT-CH, and ITO-RUT-CH composite are presented in Fig. 2. In Fig. 2a and 2b, both ITO nanoparticles and RUT have been highly dispersed in the CH matrix. Fig. 2c exhibits the ITO-RUT-CH/GCE image, evidencing the successful coating of ITO nanoparticles with RUT on the electrode's surface; Fig. 2c clearly shows that ITO nanoparticles and RUT have been well embedded in CH. The EDX studies shown in Fig. 2d confirm the presence of Ru, In-Sn, and Ru-In-Sn elementals in the corresponding composites.

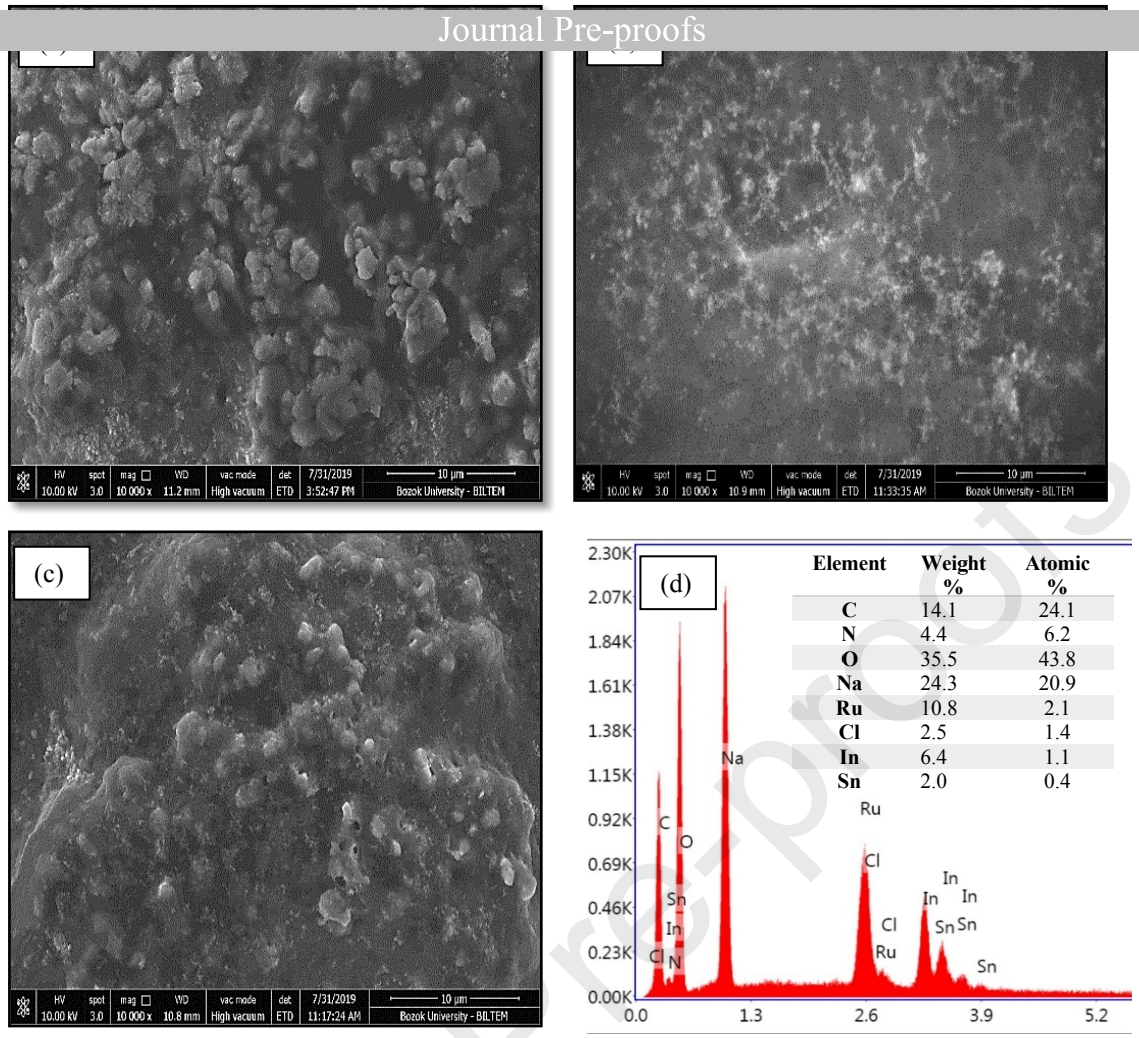

Fig. 2. SEM images of (a) ITO-CH/GCE, (b) RUT-CH/GCE, (c) ITO-RUT-CH/GCE, and EDX spectrums of (d) ITO-RUT-CH/GCE

EIS is a useful tool to characterizeof the modification process of the surface-modified electrode [49]. For this purpose, Nyquist plots of the EIS of (a) GCE, (b) ITO-CH/GCE, and (c) ITO-RUT-CH/GCE were obtained in the redox probe 5.0 mM $Fe(CN)_6^{3-/4-}$ (Fig. 3A). Nyquist plots of the imaginary impedance vs. the real impedance that expresses a semicircle part at high frequencies and a linear part at low frequencies correspond with an electron transfer-limited process and a diffusion-limited process, respectively [50, 51]. The data of EIS measurements were fitted using the Randles equivalent circuit model (inset in Fig. 3A) [49]. This circuit represents cell resistance (R_s), the charge transfer resistance of the electrode surface (R_{ct}), the constant phase element (C_{dl}), and the mass transport finite-diffusion Warburg element (Z_W) [52, 53]. R_{ct}, which is equal to the diameter of the semicircle, was calculated using the equivalent circuit fitting analysis [54]. When comparing the calculated R_{ct} values in Fig. 3A, it is clear that the R_{ct} values of ITO-CH/GCE (410 Ω) (curve b) and ITO-RUT-CH/GCE (300 Ω) (curve c) are much smaller than the bare GCEs (1050 Ω) (curve a). The reduction of R_{ct} indicates that the modified electrodes have higher electron transfer and electrical conductivity

than GCEs [29]. Curve b in Fig. 3A shows that the ITO-CH composite contributes to facilitating the electron transfer of the modified electrodes. Because the ITO nanoparticles were used together with RUT, the ITO-RUT-CH composite has the highest R_{ct} value, which is due to the synergistic effect of ITO nanoparticles and RUT.

When the ITO nanoparticles were integrated with RUT-CH/GCE surface (Fig.3B-d) and determined within the redox probe solution, the redox couple of $[Fe(CN)_6]^{3-/4-}$ clearly showed an increase compared to that of the RUT-CH/GCE (Fig.3B-b), ITO-CH/GCE (Fig.3B-c), and unmodified GCE. Fig. 3B implies that the ITO nanoparticles have been successfully modified with RUT-CH/GCE; the electron transfer of the redox probe solution at the electrode's surface was attributed to the synergistic effect of the ITO nanoparticles and RUT. Thus, it can be concluded that the ITO nanoparticles increased the conductivity of the presented biosensor by increasing the conductivity of the RUT-CH composite.

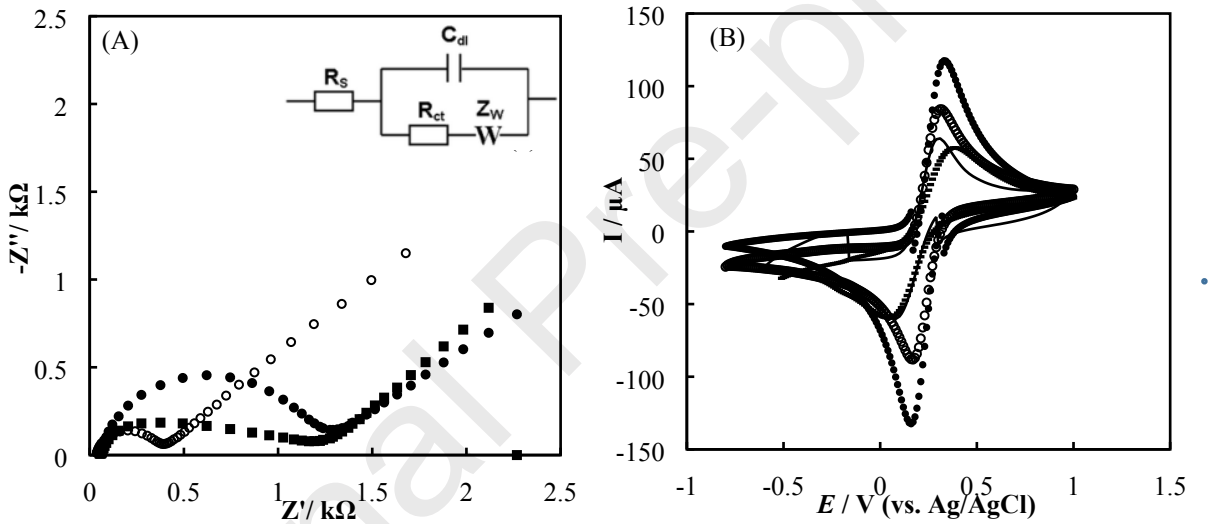

Fig. 3. (A) The Nyquist curves in (a) GCE (• • •), (b) ITO-CH/GCE (▪ ▪ ▪), and (c) ITO-RUT-CH/GCE (◦◦◦) (in 5.0 mM $Fe(CN)_6^{3-/4-}$ containing 0.5 M KCl). *Inset:* Randles equivalent circuit model, (B) CVs of (a) GCE (- - -), (b) RUT-CH/GCE (□), (c) ITO-CH/GCE (◦◦◦), (d) ITO-RUT-CH/GCE (▪ ▪ ▪) in 0.10 M KCl solution, containing 5.0 mM $Fe(CN)_6^{3-/4-}$ at a scan rate of 50 mV s^{-1}

3.2. Electrochemical behavior of modified electrodes

After studying the electrochemical characterization of the modified electrodes, it was determined that the best amperometric response of the biosensor can be achieved using the ITO-RUT-CH film-modified GCE. For this purpose, after the HRP was immobilized on the ITO-RUT-CH/GCE surface, cyclic voltammetry was used to examine the electrochemical performance and electrocatalytic response of the biosensor to H_2O_2 in PBS.

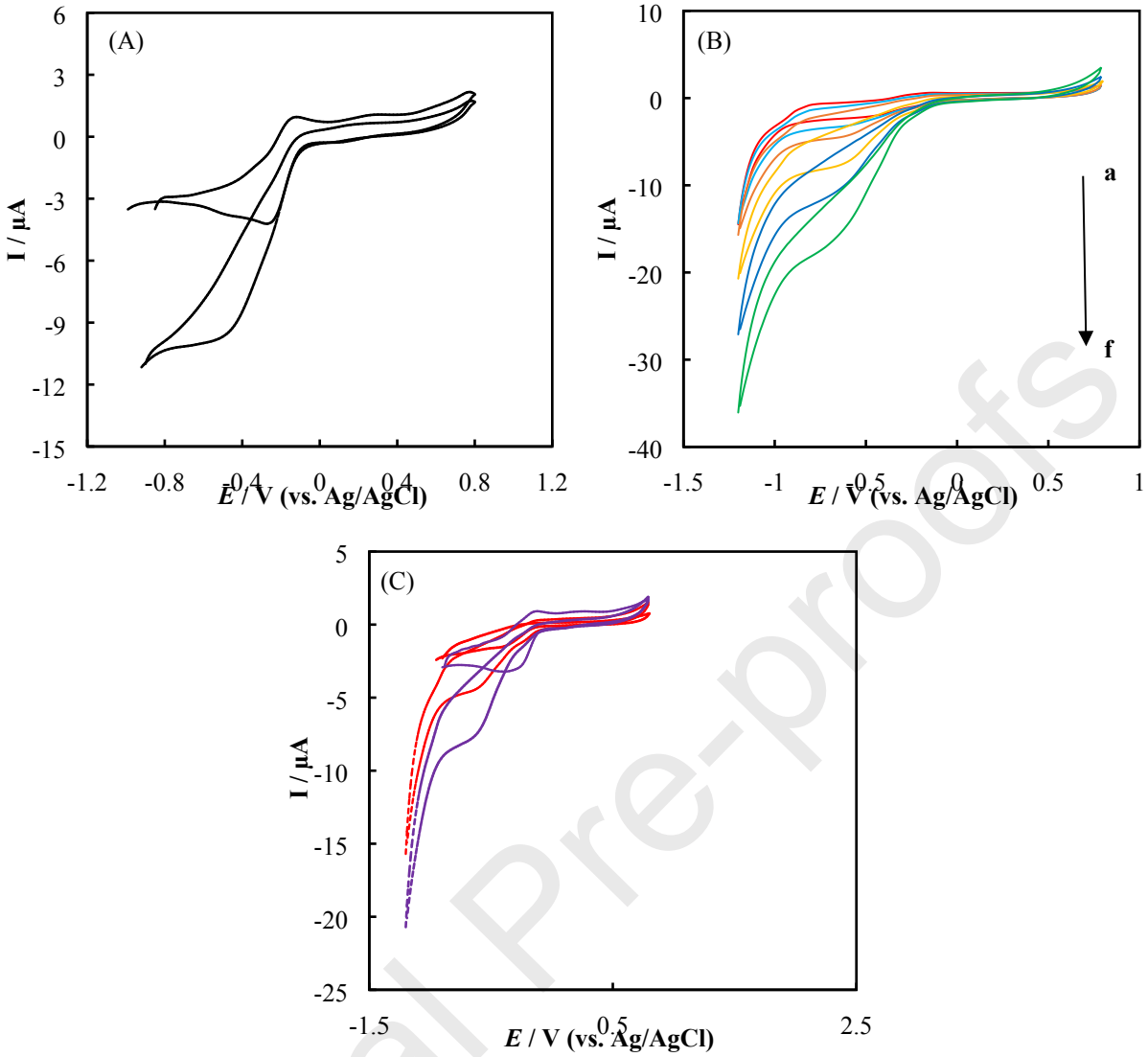

Fig. 4. (A) CVs of HRP/ITO-RUT-CH/GCE; (a) in the absence of H_2O_2 (□) and (b) in the presence of 0.5 mM H_2O_2 (- - -), (B) CVs of HRP/ITO-RUT-CH/GCE in PBS with different H_2O_2 concentrations (from a to f: 0.0, 0.05, 0.15, 0.5, 1.2, and 2.0 mM) and (C) CVs of (a,b) HRP/ITO-CH/GCE (□, - - -) and (c,d) HRP/ITO-RUT-CH/GCE (□, - - -) in PBS in the absence (a,c), and the presence (b,d) of 0.5 mM H_2O_2; scan rate: 5mVs^{-1} (in 0.05 M pH:7.5 PBS containing 0.1 M KCl).

The cyclic voltammogram (CV) of the HRP/ITO-RUT-CH/GCE, obtained in 0.05 M PBS (pH:7.5) and containing 0.1 M KCl, shows an oxidation peak at -0.15 V and a reduction peak at -0.23V. These peaks can correspond to the redox behavior of RUT. It was previously reported that RUT was used as an artificial electron acceptor [38, 55, 56].

Fig. 4A shows the CVs of the HRP/ITO-RUT-CH/GCE with and without the addition of H_2O_2. In the absence of H_2O_2, the couple peaks of RUT can only be seen from the voltammogram. When H_2O_2 is added to the above solution, the cathodic peak increases dramatically, while a reduction in the anodic peak is confirmed in the CVs. This situation

demonstrates that RUT can be catalyzed to mediate an electron transfer between H_2O_2 and the electrode surface-active center of the enzyme [57–59]. As shown in Fig. 4B, when the concentration of H_2O_2 is increased from 0.0 to 2.0 mM in the buffer solution, the catalytic current also gradually increases. The results from Fig. 4A and 4B confirm that the increased current response to H_2O_2 at the HRP/ITO-RUT-CH/GCE was obtained. These results prove that the ITO-RUT-CH nanocomposite modified electrode has strong electrocatalytic activity towards the H_2O_2 current response [60–62].

The catalytic effect of each material on the composite was studied (Fig. 4C). The ITO-CH composite was able to supply an efficient catalyze reaction. When RUT acted as a mediator for the ITO nanoparticles dispersed in CH, a better catalytic current response was shown compared to that of the HRP/ITO-CH/GCE. According to the obtained results, it is clear that RUT could play a crucial role in facilitating the rate of electron transfer between the HRP and the electrode's surface [61, 63]. The reaction mechanism of the electrocatalytic reduction of H_2O_2 is provided in Özdemir et al. [55]. RUT not only enhances electrocatalytic reaction activity but also reduces the working potential for the electrocatalytic reduction of H_2O_2 to minimize the effects of interferences [29, 38].

3.3 Optimization of ITO nanoparticles and RUT composition using the CCD model

The electrode composition was investigated to determine the high level of analytical performance shown by the biosensor. Therefore, each material on the electrode's surface modification was optimized by the 2^2 CCD model [64, 65]. In this work, the two-level factorial design was utilized for optimization. The factor levels were coded as high (+1) and low (-1) levels and a central point (0). The α value in the orthogonal and rotatable design was utilized as ±1.41. With this design, two independent variables, ITO nanoparticles and RUT, were examined at five levels with a replication at the central point using CCD. In total, 13 experiments with the HRP/ITO-RUT-CH/GCE, corresponding to all the possible combinations, were set. The amperometric current recorded at a constant H_2O_2 concentration to obtain a response for the examination of the experimental design in Supplementary Table S1.

Table 1. ANOVA of the central composite design for the optimization of ITO nanoparticles and RUT amounts

Source	Sum of squares (SS)	Degree of freedom (df)	Mean square (MS)	F-value	p-value Prob>F	
Model	1162.74	5	232.55	18.46	0.0007	significant
x_1:ITO	106.16	1	106.16	8.43	0.0229	
x_2:RUT	138.48	1	138.48	10.99	0.0128	
x_1x_2	156.25	1	156.25	12.40	0.0097	
x_1^2	561.91	1	561.91	44.60	0.0003	
x_2^2	292.78	1	292.78	23.24	0.0019	
Residual	88.19	7	12.60			
Lack of fit	70.99	3	23.66	5.50	0.0665	not significant
Pure error	17.20	4	4.30			
Cor total	1250.92	12				

To analyze the effects of parameters and their interactions, the obtained output data in the CCD was calculated by the analysis of variance (ANOVA) (Table 1). The model was evaluated with an F test for ANOVA [66]. The Probability>F-value of less than 0.05 in Table 1 indicates that the model is significant. The model F-value is 18.46 and the p-value is much smaller than 0.05, which indicates that the model is statistically significant. The lack-of-fit F-value of 5.50 and p-value of 0.0665 ($p > 0.05$) are not significant at a 95% confidence level, indicating that the model is acceptable for the experimental data. The results obtained in 2^2 CCD presented that the model terms of x_1, x_2, x_1x_2, x_1^2, and x_2^2 are described as significant factors at a 95.0% confidence level.

The coefficient of determination (R^2) value was determined as 0.9295. This value was an acceptable regression between experimental and predicted values. The second-order model [Eq. (3)] in coded form was designed based on analysis of the data in Table 1 (x_1:ITO; x_2:RUT):

$$\hat{y} = 43.60 - 3.64\,x_1 + 4.16\,x_2 - 8.99\,x_1^2 - 6.49\,x_2^2 - 6.25\,x_1x_2 \quad (3)$$

Fig. 5 shows the three-dimensional (3D) response surface plots related to the interaction of factors on the amperometric current response result. One of the factors was changed and the other one was fixed; the optimum factor was determined according to the obtained highest current response. When ITO nanoparticles or RUT amounts are increased, the current response is also enhanced. Further increasing the amount of ITO nanoparticles or RUT causes a reduction in the biosensor's response, indicating a strong relationship between the variables and the amperometric response current. The optimum amperometric response was obtained with 5.9 ITO mg/mL and 3.4 RUT mg/mL. The optimum values obtained are used in all experiments.

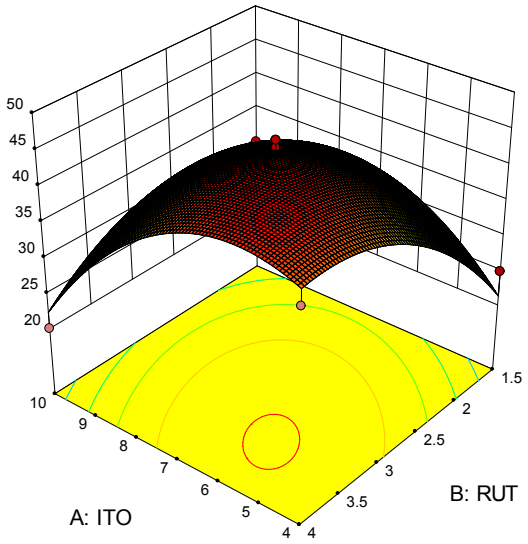

Fig. 5. 3D response surface plots of peak current as a function of A: ITO nanoparticles and B: RUT amounts

3.4 Amperometric response to H_2O_2

After obtaining the optimum electrode composition results, amperometric studies were performed at room temperature and stirred in 0.05 M PBS at the applied potential of -0.25V vs. Ag/AgCl. Fig. S1-A shows the amperometric responses of the (a) HRP/ITO-RUT-CH/GCE, (b) HRP/ITO-CH/GCE, and (c) HRP/GCE, examined by the successive addition of H_2O_2 aliquots to the buffer solution. When the calibration plots of these biosensors were compared, the sensitivity of the HRP/ITO-RUT-CH/GCE was approximately 1.5 times higher than that of the HRP/ITO-CH/GCE and 3.5 times higher than of the HRP/GCE. The best sensitivity was obtained with both ITO nanoparticles and RUT. The HRP/ITO-RUT-CH/GCE response to H_2O_2 was linear between 0.05 and 0.72 mM with a sensitivity of 7.5 μAmM^{-1} cm^{-2} (0.53 $\mu A/mM$). The LOD of the biosensor was found to be 0.008 mM for the HRP/ITO-RUT-CH/GCE. The LOD values are better than those of most bio(sensors) reported in the literature. When the catalase enzyme was immobilized onto the GCE surface by crosslinking with glutaraldehyde and BSA [17], the biosensor exhibited a low sensitivity of 1.23 $\mu AmM^{-1}cm^{-2}$ with a detection limit of 0.28 mM for H_2O_2. Yang et al. [67] proposed an H_2O_2 inhibition biosensor based on a cysteamine self-assembled monolayer modified Au electrode, with a LOD of 0.2 mM. Al-Hardan et al. [68] improved a non-enzymatic H_2O_2 sensor based on zinc oxide nanorods; the LODs were found to be 0.04mM and 0.1435 mM, respectively. The immobilization of the HRP on the electrodes modified with Au-thin-film gold showed a detection limit of 0.016 mM [69]. Yuan et al. [70] developed the chitosan/2D layered double hydroxide composite biosensor with a detection limit of 0.0128 mM. The H_2O_2

bioelectrochemical sensor prepared $CoMn_2O_4$ nanoparticle modified graphite in a LOD of 0.04 mM [71].

3.5 Optimization of experimental parameters for inhibition

3.5.1 Influence of H_2O_2 concentration

The degree of enzyme inhibition was investigated by assessing the HRP activity at different H_2O_2 concentrations; this is because the response of the biosensor can vary between high and low substrate concentration levels. The influence of substrate concentration was tested at different levels between 0.25 mM and 1.0 mM H_2O_2 (Fig. S2-A). When the concentration of H_2O_2 was lower than 0.75 mM, the biosensor response was not sufficiently discernable and was almost equal to the inhibition by Pb^{2+}. However, when the substrate concentration was too high, the degree of inhibition decreased due to a blockage in the enzyme active center [34, 65]. Therefore, a concentration of 0.75 mM H_2O_2 was selected as the optimum substrate concentration to obtain the best results. The inhibition degree increased with the increasing levels of a substrate; these results are in concordance with the literature reports [72].

The apparent Michaelis–Menten constant (K_m^{app}), which shows the improved catalytic activity of the HRP to H_2O_2, was calculated using the Lineweaver–Burk equation (Fig. S1-B) [73]. The value K_m^{app} was found to be 0.23 mM for the HRP/ITO-RUT-CH/GCE. This value is lower than those of previously reported studies [19, 42, 62, 67, 74, 75]. The concentration of H_2O_2 also corresponds with 0.75 mM ($>2\,K_m^{app}$), which was used to evaluate the maximum activity of the HRP before and after inhibition [76]. The optimum concentration was selected as 0.75 mM for further studies.

3.5.2 Influence of enzyme amounts, pH, and working potential

The amount of enzyme is an important parameter that influences the enzymatic activity of the biosensor [17, 40]. Hence, in this study, to investigate the effect of enzyme amounts on enzymatic activity under inhibition circumstances, different HRP concentrations (1.0–30.0 mg/mL HRP) were used for biosensor construction (Fig. S2-B). The optimization of enzyme loading was evaluated using different HRP-immobilized electrodes; this was done after adding heavy metals (Pb^{2+}, Ni^{2+}, Cd^{2+}) as an inhibitor, in the presence of a constant concentration of H_2O_2 (0.75 mM). As shown in Fig. S2-B, when the amount of HRP increases, the degree of inhibition increases to 8.0 mg/mL HRP. The highest degree of inhibition was found to be 8.0 mg/mL HRP immobilized on the ITO-RUT-CH/GCE surface; this concentration was used in further studies.

The pH value has a significant role in the selectivity of the biosensor and enzyme inhibition, because enzyme activity is highly dependent on pH [77]. An optimum pH was examined within a range of 6.0–9.0 in the presence of 0.1 mM Pb^{2+} (Fig. S2-C). As shown in Fig. S2-C, the amperometric current response increases with the pH level, until the pH is 6.5, and is then reduced. It is known that OH^- ions participate in the reaction between RUT and H_2O_2. This current change was linked to the change in RUT structure of the acidic and basic medium [55]. So, the optimum pH for the inhibition of the enzyme electrode was pH 6.5.

To investigate the influence of working potential on the amperometric response of the HRP/ITO-RUT-CH/GCE, the biosensor response towards H_2O_2 was recorded at different applied potentials between -0.10 and -0.30 (Fig. S2-D) due to the anodic and cathodic peaks of RUT (Fig. 4A). The maximum amperometric response was obtained at -0.30 V, but the lower working potential of -0.25 V vs. Ag/AgCl was selected to reduce the effects of interference species in real samples [42].

3.6 Performance parameters of the HRP/ITO-RUT-CH/GCE inhibition biosensor

3.6.1 Inhibition studies of Pb^{2+}, Ni^{2+}, and Cd^{2+}

Heavy metals, used as an inhibitor of the HRP, have been previously reported in the literature [17, 19, 36, 40, 42, 78, 79]. To determine the inhibitory effect of Pb^{2+}, Ni^{2+}, and Cd^{2+} ions, the CVs of the HRP/ITO-RUT-CH/GCE were examined at different stages (Fig. 6). The CVs of the biosensor were observed in 0.05 M PBS with and without the addition of 0.75 mM H_2O_2 (Fig. 6a-b). Fig. 6c shows that adding 10^{-4} M Pb^{2+} causes the catalytic current to reduce significantly.. This indicates that heavy metals inhibited the HRP effectively. It was concluded that the HRP/ITO-RUT-CH/GCE could be used to evaluate the concentration of heavy metal ions by inhibition [62, 80].

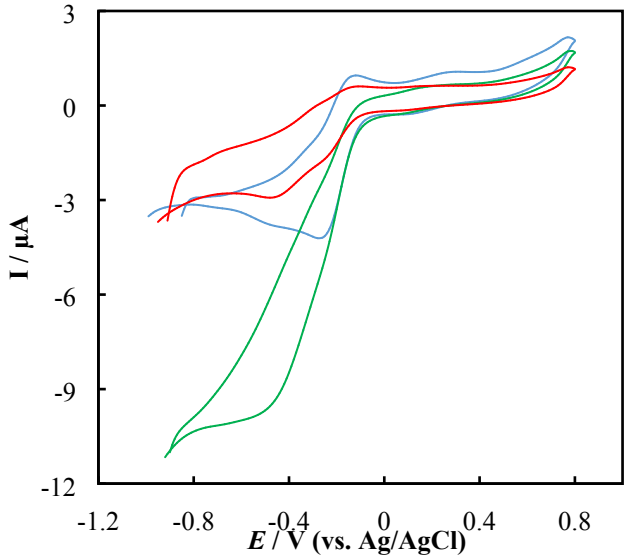

Fig. 6. CVs of the HRP/ITO-RUT-CH/GCE (a) the electrode in 0.05 M PBS (blue line) (b) the same as (a) containing 0.75mM H_2O_2 (green line); (c) the same as (b) with 10^{-4} M 100 µL Pb^{2+} added (red line); scan rate: 5mVs^{-1} (in 0.05 M pH:7.5 PBS containing 0.1 M KCl).

The mechanism and constant of inhibition were achieved using Dixon plots [81] and Cornish-Bowden plots [82] at three different concentrations of each of the heavy metal ions (Pb^{2+}, Ni^{2+}, Cd^{2+}) (Fig. 7). The type of enzyme inhibition and dissociation constant of the enzyme–inhibitor substrate complex (K_i') of each metal was determined from Fig. 7. The three parallel lines in the Dixon plots (Fig. 7 A1, A2, and A3) indicated the uncompetitive inhibition of the HRP by Pb^{2+}, Ni^{2+}, and Cd^{2+}.

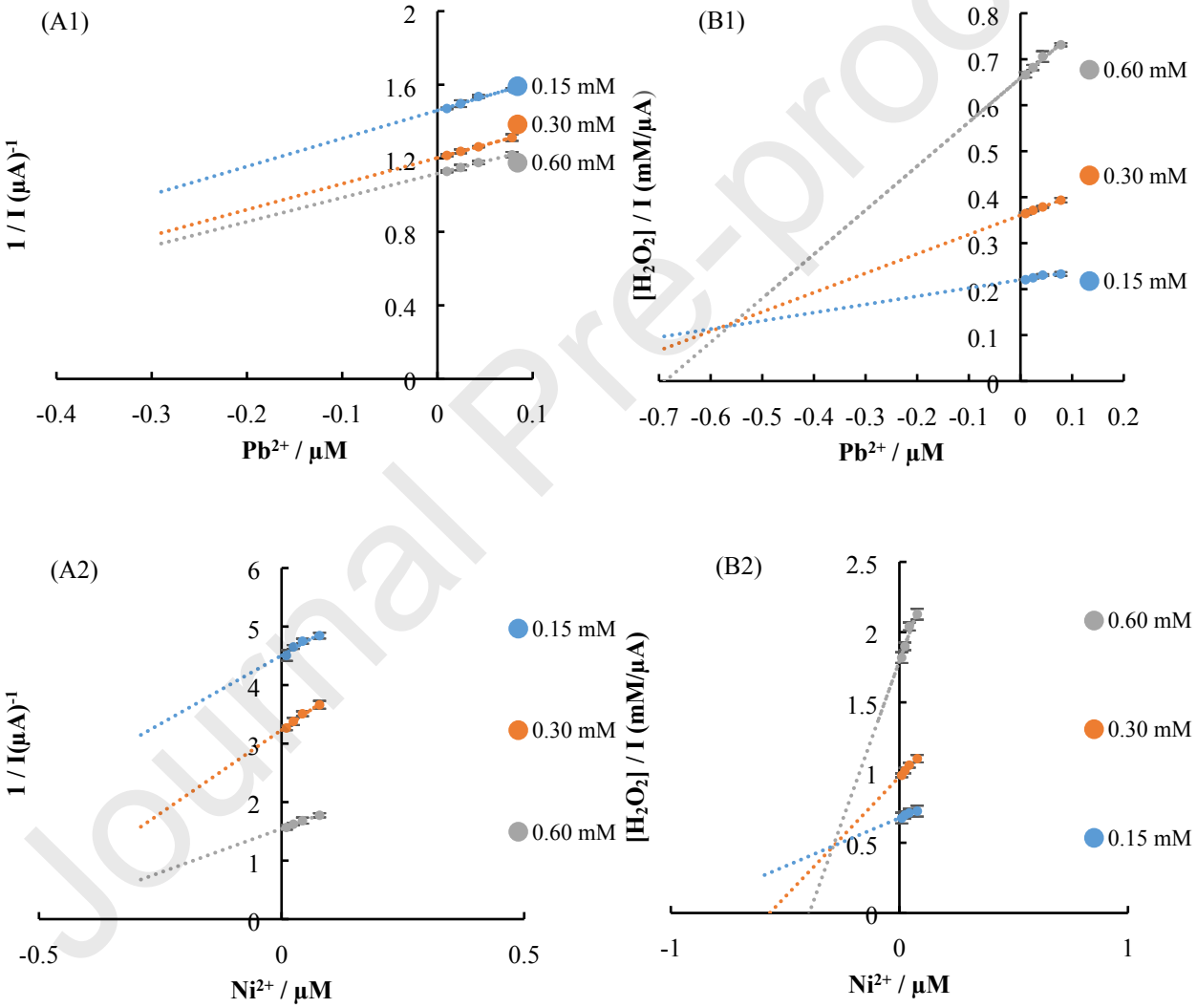

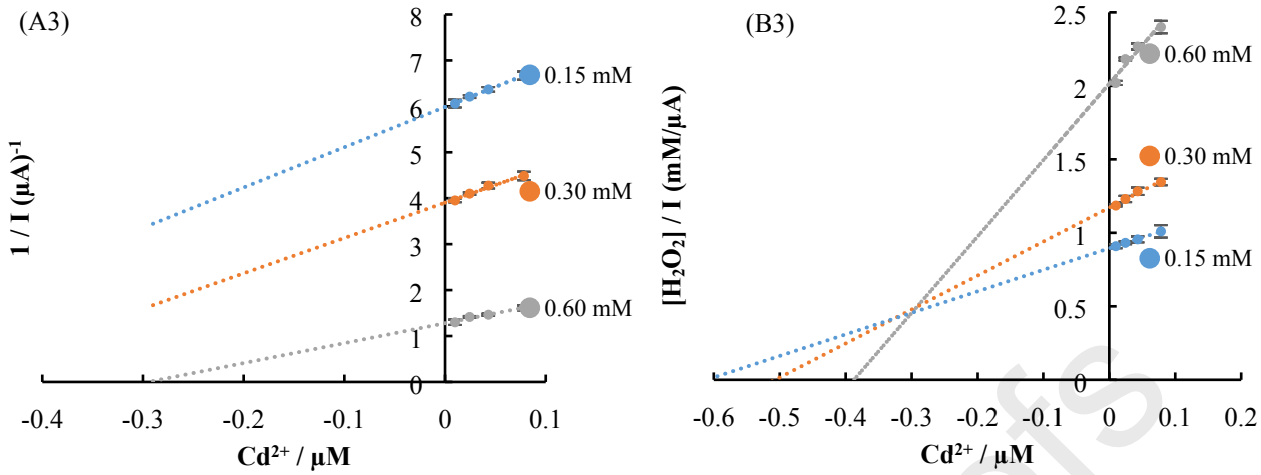

Fig. 7. (A) The Dixon plots and (B) Cornish-Bowden plots of the effect of Pb^{2+} (A1, B1); Ni^{2+} (A2,B2) and Cd^{2+} (A3, B3) three different concentrations of H_2O_2 (0.15; 0.30 and 0.60 mM) on the HRP (error bars represent the standard deviation of three measurements).

The Cornish-Bowden plot (Fig. 7 B1, B2, and B3) shows that the inhibition is uncompetitive because the three lines intercept in the second quadrant of the x-axis. From an evaluation of the two plots, it was confirmed that the mechanism of inhibition is uncompetitive. In this type of inhibition, an enzyme inhibitor, Pb^{2+}, Ni^{2+}, or Cd^{2+}, binds only to the enzyme-substrate complex. The resulting complex (enzyme-substrate-inhibitor) binds to the enzyme irreversibly and inhibits the activity of the enzyme. Thus, a decrease in amperometric response is observed after the addition of the inhibitor [82, 83]. The calculated $K_i^{'}$ values for three metal ions are 0.56 µM (Pb^{2+}), 0.29 µM (Ni^{2+}), and 0.27 µM (Cd^{2+}). The uncompetitive inhibition of the HRP by $Pb^{2+}$and Cd^{2+} confirms the obtained data in the literature reports [19, 40].

The amperometric response of the HRP/ITO-RUT-CH/GCE to Pb^{2+}, Ni^{2+} and Cd^{2+} with the addition of 0.75 mM H_2O_2 was investigated under optimized working conditions (Fig. 8A). The curve in Fig. 8A indicates that the degree of the HRP inhibition increased with the rising concentrations of heavy metal ions. The curve in Fig. 8B, C and D show the biosensor's amperometric response (*i*–t) to these heavy metals. The concentration of added heavy metal ions (Pb^{2+}, Ni^{2+} or Cd^{2+}) lead to the inhibition of enzyme activity, so a decrease in current was observed [36]. The inhibition calibration curves of the HRP/ITO-RUT-CH/GCE were performed within the range of 0.009–0.301 µM with a LOD of 8 nM for Pb^{2+}, 0.011–0.368 µM with a LOD of 3 nM for Ni^{2+}, and 0.008-0.372 µM with a LOD of 1 nM µM for Cd^{2+} (Fig. S3). The LOD of the biosensor was found to have a signal-to-noise ratio of 3 and was calculated according to the 3sb/m criterion,, where m is the slope of the lowest calibration graph and s_b is

the standard deviation (n = 10) of the signals from 0.009 µM, 0.011 µM, and 0.0077 µM for Pb^{2+}, Ni^{2+}, and Cd^{2+}, respectively [84, 85].

In this study, the sensitivity values were calculated from the calibration curves and determined to be $^{+}$ 11.97 $\mu A \mu M^{-1} cm^{-2}$ (0.85 $\mu A \mu M^{-1}$), 10.84 $\mu A \mu M^{-1}$ cm^{-2} (0.77 $\mu A \mu M^{-1}$), and 10.99 $\mu A \mu M^{-1} cm^{-2}$ (0.78 $\mu A \mu M^{-1}$) for Pb^{2+}, Ni^{2+}, and Cd^{2+}, respectively. The obtained sensitivity values are better than most of the inhibition biosensors in the literature reports. Guascito et al. [48], enhanced an inhibition biosensor with a sensitivity of 0.229 $\mu A \mu M^{-1} cm^{-2}$ for Cd^{2+} and 0.051 $\mu A \mu M^{-1} cm^{-2}$ for Ni^{2+}. GOx enzyme inhibition sensors prepared cobalt or copper hexacyanoferrate modified carbon film electrodes with a sensitivity of 17.6 $nA \mu M^{-1} cm^{-2}$ for Cd^{2+} and 0.75 $nA \mu M^{-1} cm^{-2}$ Ni^{2+} [86]. Ayenimo et al. [87] developed the ultrathin PPy-GOx biosensor with a sensitivity of 1.0 $\mu A \mu M^{-1} cm^{-2}$ for Pb^{2+} and 0.50 $\mu A \mu M^{-1} cm^{-2}$ for Cd^{2+}. Gumpu et al. [88] showed an inhibition biosensor with a sensitivity of 124.7 $\mu A \mu M^{-1} cm^{-2}$ for Cd^{2+}.

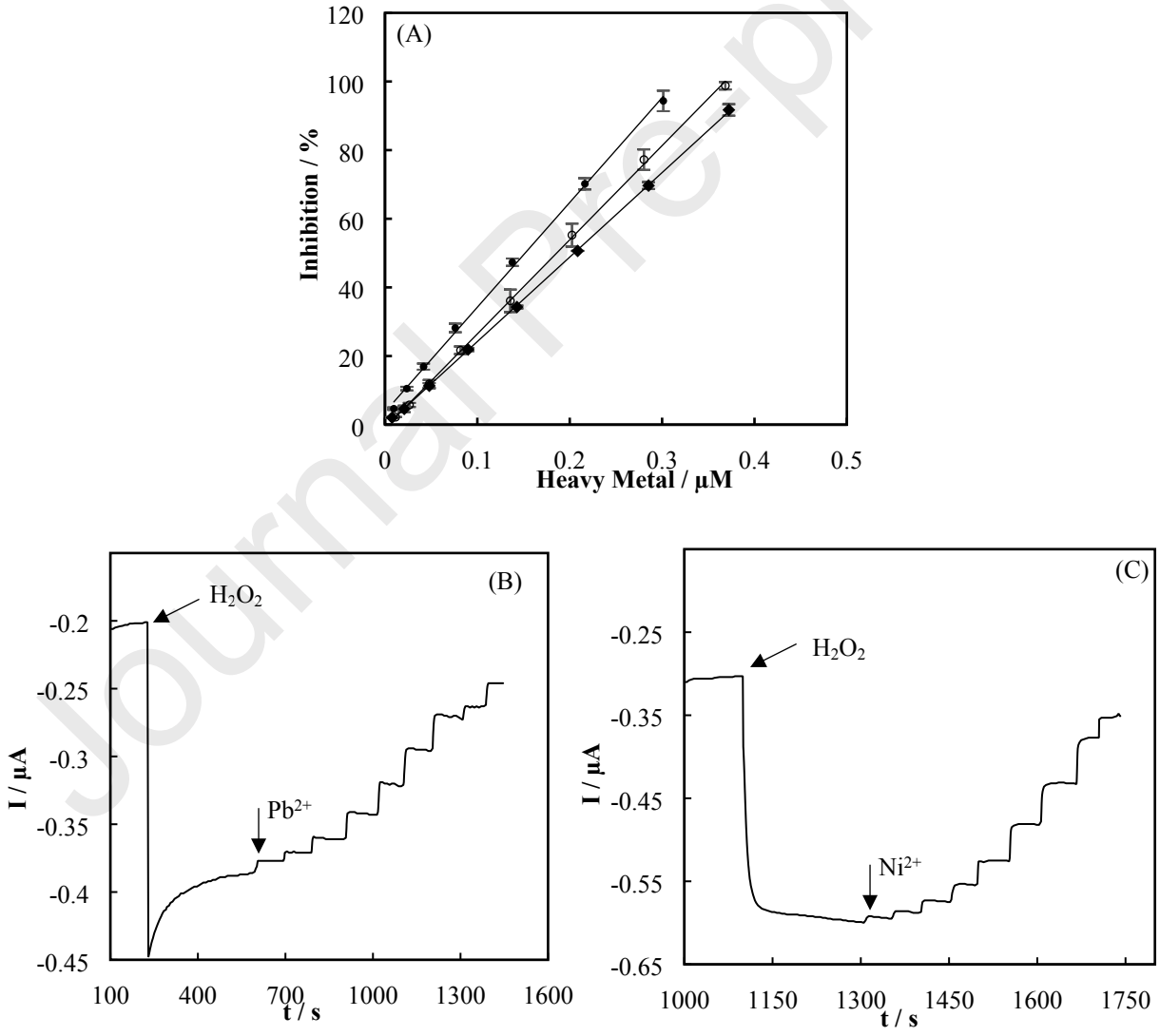

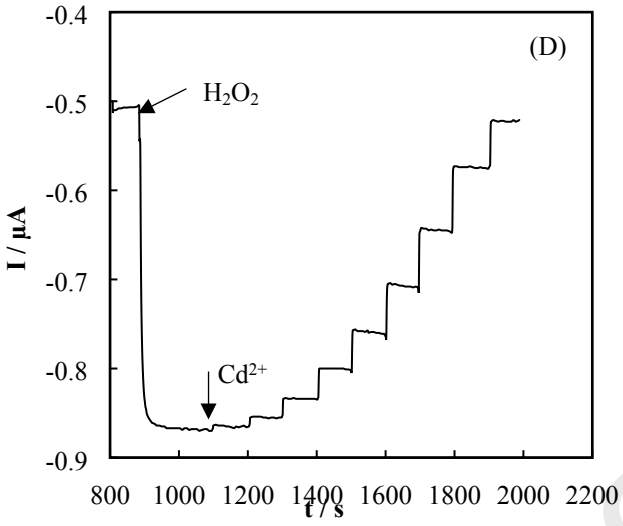

Fig. 8. (A) Inhibition calibration curve for the determination of (a)Pb^{2+} (• • •), (b)Ni^{2+} (◦ ◦ ◦), and (c)Cd^{2+} (♦ ♦ ♦) with the addition of 0.75 mM H_2O_2 (error bars represent the standard deviation of three measurements). Chronoamperometric response to (B) Pb^{2+}, (C) Ni^{2+} and (D) Cd^{2+} at HRP/ITO-RUT-CH/GCE inhibition biosensor. Applied potential of -0.25V vs. Ag/AgCl (in 0.05 M pH:6.5 PBS).

Table 2. Analytical performance characteristics of an enzyme inhibition-based amperometric biosensor for the determination of Pb^{2+}, Ni^{2+}, and Cd^{2+}

Biosensor composition	*Heavy metal*	*Inhibition type*	*Applied potential/ pH*	*Linear range, nM*	*LOD, nM*	*Ref.*
PQQ-GDH	Cd^{2+} Pb^{2+}	non-competitive	+0.25 V/6.0	$1.5x10^5$–$1.5x10^6$ $1.5x10^5$–$3.5x10^6$	$1.5x10^4$	[89]
SPE/urease-glutamic dehydrogenase	Cd^{2+} Pb^{2+}	-	+0.30 V/8.0	$8.9x10^2$–$2.7x10^5$ ND	$2.5\ x10^3$ ND	[90]
Pt/PPD/GOx	Cd^{2+} Ni^{2+}	-	+0.70 V/7.0	$2\ x10^4$-$1.5\ x10^5$ $3.5\ x10^4$-$4.4\ x10^5$	3000 4800	[48]
Pt-UME/Sucrose	Cd^{2+} Pb^{2+}	reversible irreversible	+0.35 V/5.5	25–125 50–250	25 30	[91]
Screen-printed seramic electrode/Urease	Cd^{2+}	-	+0.28 V/8.1	0–178	-	[92]
PANI-HRP	Cd^{2+} Pb^{2+}	non-competitive	-0.20 V/7.02	42-490 23-270	0.8 0.2	[42]
CoHCF/GOx CuHCF/GOx	Cd^{2+} Ni^{2+}	competitive	-0.45 V/7.0 -0.35V/7.0	1500-6000 $20000\text{-}1.2x10^3$	1200 4800	[86]
HRP/MT-MWCNT	Pb^{2+}	reversible mixed	-0.30 V/7.0	440–2650	12	[79]
PPy-GOx	Cd^{2+} Pb^{2+}	competitive mixed	+0.70 V/7.0	4000–26000 1600–7700	4000 1600	[87]
GOx/PBG_{DES}/MWCNT	Cd^{2+} Pb^{2+}	competitive uncompetitive	-0.40 V/7.0	10–80 10–120	1.75 2.70	[40]
GOx–Nb–SWCNT	Pb^{2+}	competitive	+0.58 V/7.0	3000–25000	-	[93]

GOx/Co_3O_4	Pb^{2+} Ni^{2+} Cd^{2+}	competitive	+0.50 V/7.0	2413–36198 8519–161867 4447–111199	241 851 445	[94]
Ru(II)-tris(bipy)-GO/AChE	Cd^{2+}	competitive and mixed inhibition	+0.223 V/6.0	20–700	70	[88]
ChOx/MWCNT	Pb^{2+}	competitive	-0.35 V/8.5	0.1–10	0.04	[95]
HRP/ITO-RUT-CH	Pb^{2+} Ni^{2+} Cd^{2+}	uncompetitive	-0.25 V/6.5	9.6–301 11–368 7.7–372	8.0 3.0 1.0	This work

MT-MWCNT:maize tassel multiwalled carbon nanotube; CoHCF: cobalt hexacyanoferrate; CuHCF: copper hexacyanoferrate; GOx: glucose oxidase enzyme; PANI: poly(aniline); PPy: polypyrrole; PBG_{DES}: poly(brilliant green)–deep eutectic solvent; PQQ:pyrroloquinoline quinone; GDH: glucose dehydrogenase; UME:Ultra-microelectrode; PPD: poly-o-phenylenediamine; SPE:scree-printed electrode; Nb–SWCNT: single-walled carbon nanotubes/Nile blue; RuO_2: ruthenium(IV) oxide; GO: graphene oxide; AChE:acetylcholineesterase; ChOx: choline oxidase; ND: not detected.

3.6.2 Performance parameters

The interference effect of possible species (Ca^{2+}, Mg^{2+}, Zn^{2+}, Na^{+}, K^{+}, Fe^{2+}, Hg^{2+}, and Mn^{2+}) on the biosensor response was tested in the tap water matrix. For the assay of each of the metal ions (Pb^{2+}, Ni^{2+}, and Cd^{2+}), it was observed that there was no important effect on the initial response of analytes in the presence of 20-fold Ca^{2+}, Mg^{2+}, Zn^{2+}, Na^{+}, and K^{+} (less than 10%). Similarly, no significant influence on the biosensor response was observed in the presence of two-fold Fe^{2+}, Hg^{2+}, or Mn^{2+} interference species (less than 10%). The stability and reproducibility of the HRP/ITO-RUT-CH/GCE were investigated under optimized inhibition circumstances. The stability of the biosensor was evaluated by measuring the response of Pb^{2+}, Ni^{2+}, and Cd^{2+} in the presence of 0.75 mM H_2O_2. After two weeks, the biosensor lost only 19%, 13%, and 11% of the initial response towards Pb^{2+}, Ni^{2+}, and Cd^{2+}, respectively. It is thought that the stability of biosensor decreases after two weeksdue to the reduction in the activity of the enzyme after each measurement. Following each measure, the biosensor was dipped in a 0.5-mM EDTA solution to regenerate within 100 s[13]. When the biosensor was not used, it was stored at 4°C. The five electrodes were prepared in the same manner utilized for the reproducibility of the biosensor. The relative standard deviation (RSD) value was found to be 4.2% for Pb^{2+}, 1.6% for Ni^{2+}, and 3.8% for Cd^{2+}. The results revealed that the biosensor showed good selectivity, stability, and reproducibility for Pb^{2+}, Ni^{2+}, and Cd^{2+}. All biosensors responded rapidly to changes in the Pb^{2+}, Ni^{2+}, and Cd^{2+}concentration, reaching 95% of the steady-state current in less than 10 s. Moreover, the Nafion layer contributed to the stability of the electrode by preventing the enzyme from leaking [35].

3.6.3 Application of the biosensor

The applicability of the enzyme inhibition biosensor for the determination of Pb^{2+}, Ni^{2+}, and Cd^{2+} in tap water was demonstrated by the standard addition method. The tap water sample

was also assayed using AAS. The results of the AAS showed that the levels of Pb^{2+}, Ni^{2+}, and Cd^{2+} were below the detection limit in the water sample taken from the tap. Therefore, a tap water sample was prepared with the addition of 9.53 ppm Pb^{2+}, 2.98 ppm Ni^{2+}, and 4.83 ppm Cd^{2+}. Standard addition method was used to determine the content of each metal ion in spiked tap water sample. Tap water sample was spiked with four different concentrations of standard metal solution of Pb^{2+}, Ni^{2+} or Cd^{2+} and a multiple addition calibration curve was obtained. The concentration for each heavy metal ion concentration in spiked sample was calculated from this calibration curve, Table 3. The maximum allowed limits of Pb^{2+}, Ni^{2+}, and Cd^{2+} in drinking water have been specified by the WHO [4]. The developed biosensor was able to determine the concentration of heavy metals below the maximum contaminant levels presented by the WHO. The recovery values were obtained, and the results are shown in Table 3. The results obtained by the proposed biosensor method and AAS were statistically compared by a t-test at a 95% confidence level. Table 3 shows that the obtained $t_{critical}$ value is higher than the t value. When the results obtained from both methods were compared, there was no statistically significant difference. This phenomenon showed that the presented biosensor could be applied to the detection of Pb^{2+}, Ni^{2+}, and Cd^{2+} in real water samples.

Table 3. Recovery of Pb^{2+}, Ni^{2+}, and Cd^{2+} in a tap water sample

		Amperometric Biosensor			**AAS**			
Heavy Metal	Levels present (ppb) AAS	Added (ppb)	Found (ppb)	Recovery (%)	Added (ppb)	Found (ppb)	Recovery (%)	t
Pb^{2+}	ND	9.53	9.37 ± 0.46	98.3 ± 4.7	9.53	9.41 ± 0.39	101.8 ± 9.8	0.30
Ni^{2+}	ND	2.98	3.04 ± 0.14	102.0 ± 4.8	2.98	2.91 ± 0.37	97.6±12.1	2.12
Cd^{2+}	ND	4.83	4.83 ± 0.18	99.8 ± 3.7	4.83	4.98 ± 0.20	104.8 ± 9.5	1.52

* Results are expressed as $\bar{x} \pm \frac{ts}{\sqrt{N}}$ (for n=3, $t_{critical}$=2.78); ND: not detected.

4. Conclusions

An amperometric biosensor for the determination of Pb^{2+}, Ni^{2+}, and Cd^{2+}, based on the inhibition of the HRP, was successfully developed using ITO-RUT-CH film modified GCE. The ITO-RUT-CH film exhibited a synergistic catalytic effect between the ITO nanoparticles and RUT, which can be attributed to the facilitation of the electron transfer between the active center of the HRP and the electrode's surface. The amount of ITO nanoparticles and RUT were optimized through a central composite design, with founding values of 5.9 mg/mL for ITO nanoparticles and 3.4 mg/mL for RUT. The HRP/ITO-RUT-CH/GCE inhibition biosensor showed good analytical performance, such as fast response, good operational stability, high reproducibility, good selectivity and sensitivity, and low detection limit, compared with those

in the literature. The inhibition of the HRP/ITO-RUT-CH/GCE biosensor in the presence of sequential aliquots Pb^{2+}, Ni^{2+}, and Cd^{2+} were examined in tap water for the first time. The HRP inhibition biosensor allowed good sensitivity and the selective analysis of Pb^{2+}, Ni^{2+}, and Cd^{2+} in a tap water matrix, which indicated that the proposed biosensor could be used as a promising analytical approach for monitoring trace metals in different water sources. Furthermore, because the enzyme electrode showed a superior electrocatalytic reduction in H_2O_2, the biosensor can be used as an alternative for the determination of H_2O_2 compared with other reported H_2O_2 bio(sensors).

Acknowledgments

The author thankfully acknowledges Prof. Dr. Orhan ATAKOL and Erdal EMİR (Ankara University, Department of Chemistry) for the AAS analysis.

References

[1] G. Shtenberg, N. Massad-Ivanir, E. Segal, Detection of trace heavy metal ions in water by nanostructured porous Si biosensors, Analyst 140(13) (2015) 4507-4514.
[2] J.O. Duruibe, M. Ogwuegbu, J. Egwurugwu, Heavy metal pollution and human biotoxic effects, International J. Phys. Sci. 2(5) (2007) 112-118.
[3] M. Kucuk, I. Gulcin, Purification and characterization of the carbonic anhydrase enzyme from Black Sea trout (Salmo trutta Labrax Coruhensis) kidney and inhibition effects of some metal ions on enzyme activity, Environ. Toxicol. Phar. 44 (2016) 134-139.
[4] G. WHO, Guidelines for drinking-water quality, World Health Organization 216 (2011) 303-4.
[5] D. dos Santos Silva, C.S. dos Santos, L.A. Pando, M.S.R. Gomes, C.G. Novaes, WN.L. dos Santos, M.A. Bezerra, Doehlert design in the optimization of ultrasound assisted dissolution of fish fillet samples with tetramethyl ammonium hydroxide for metals determination using FAAS, Food Chem. 273 (2019) 71-76.
[6] M. Safari, Y. Yamini, M.Y. Masoomi, A. Morsali, A. Mani-Varnosfaderani, Magnetic metal-organic frameworks for the extraction of trace amounts of heavy metal ions prior to their determination by ICP-AES, Microchim. Acta 184(5) (2017) 1555-1564.
[7] G. Okano, S. Igarashi, Y. Yamamoto, S. Saito, Y. Takagai, T. Ohtomo, S. Kimura, O. Ohno, Y. Oka, HPLC-spectrophotometric detection of trace heavy metals via 'cascade'separation and concentration, Int. J. Environ. An. Ch. 95(2) (2015) 135-144.
[8] D. Zhang, Q. Liu, Biosensors and bioelectronics on smartphone for portable biochemical detection, Biosens. Bioelectron. 75 (2016) 273-284.
[9] S. Vigneshvar, C. Sudhakumari, B. Senthilkumaran, H. Prakash, Recent advances in biosensor technology for potential applications–an overview, Front. bioeng. biotechnol. 4 (2016) 11.
[10] L. Qiana, X. Yanga, Composite film of carbon nanotubes and chitosan for preparation of amperometric hydrogen peroxide biosensor, Talanta 68(3) 721-727.
[11] L. Eggeling, M. Bott, J. Marienhagen, Novel screening methods—biosensors, Curr. Opin. Biotech. 35 (2015) 30-36.

[12] A. Amine, H. Mohammadi, I. Bourais, G. Palleschi, Enzyme inhibition-based biosensors for food safety and environmental monitoring, Biosensors and Bioelectronics 21(8) (2006) 1405-1423.
[13] C. Malitesta, M. Guascito, Heavy metal determination by biosensors based on enzyme immobilised by electropolymerisation, Biosens. Bioelectron. 20(8) (2005) 1643-1647.
[14] R. Ilangovan, D. Daniel, A. Krastanov, C. Zachariah, R. Elizabeth, Enzyme based biosensor for heavy metal ions determination, Biotechnology & Biotechnological Equipment 20(1) (2006) 184-189.
[15] S. Oliveira, O. Corduneanu, A. Oliveira-Brett, In situ evaluation of heavy metal–DNA interactions using an electrochemical DNA biosensor, Bioelectrochem. 72(1) (2008) 53-58.
[16] O. Syshchyk, V.A. Skryshevsky, O.O. Soldatkin, A.P. Soldatkin, Enzyme biosensor systems based on porous silicon photoluminescence for detection of glucose, urea and heavy metals, Biosens. Bioelectron. 66 (2015) 89-94.
[17] B. Elsebai, M.E. Ghica, M.N. Abbas, C.M. Brett, Catalase based hydrogen peroxide biosensor for mercury determination by inhibition measurements, J. Hazard. Mater. 340 (2017) 344-350.
[18] O. Domínguez-Renedo, M. Alonso-Lomillo, L. Ferreira-Goncalves, M. Arcos-Martínez, Development of urease based amperometric biosensors for the inhibitive determination of Hg (II), Talanta 79(5) (2009) 1306-1310.
[19] B. Silwana, C. Van Der Horst, E. Iwuoha, V. Somerset, Amperometric determination of cadmium, lead, and mercury metal ions using a novel polymer immobilised horseradish peroxidase biosensor system, J. Environ. Sci. Heal. A. 49(13) (2014) 1501-1511.
[20] M. Dequaire, B. Limoges, J. Moiroux, J.M. Savéant, Mediated electrochemistry of horseradish peroxidase.Catalysis and inhibition. J. Am. Chem. Soc. 124(2) (2002) 240-253.
[21] A. Mahmoudi, K. Nazari, N. Mohammadian, A.A. Moosavi-Movahedi, Effect of Mn^{2+}, Co^{2+}, Ni^{2+}, and Cu^{2+} on horseradish peroxidase. Appl. Biochem. Biotech. 104(1) (2003). 81-94.
[22] M. Holzinger, A. Le Goff, S. Cosnier, Nanomaterials for biosensing applications: a review, Front. Chem. 2 (2014) 63.
[23] S. Chen, R. Yuan, Y. Chai, F. Hu, Electrochemical sensing of hydrogen peroxide using metal nanoparticles: a review, Microchim. Acta 180(1-2) (2013) 15-32.
[24] X. Luo, A. Morrin, A.J. Killard, M.R. Smyth, Application of nanoparticles in electrochemical sensors and biosensors, Electroanalysis, Electroanal. 18(4) (2006) 319-326.
[25] E.B. Aydın, M.K. Sezgintürk, Indium tin oxide (ITO): A promising material in biosensing technology, TRAC-Trend. Anal. Chem. 97 (2017) 309-315.
[26] M.Z.H. Khan, Effect of ITO surface properties on SAM modification: A review toward biosensor application, Cogent Eng. 3(1) (2016) 1170097.
[27] P. Sivasakthi, G.R. Bapu, M. Chandrasekaran, Pulse electrodeposited nickel-indium tin oxide nanocomposite as an electrocatalyst for non-enzymatic glucose sensing, Mater. Sci. Eng. C 58 (2016) 782-789.
[28] F. Rigoni, G. Drera, S. Pagliara, A. Goldoni, L. Sangaletti, High sensitivity, moisture selective, ammonia gas sensors based on single-walled carbon nanotubes functionalized with indium tin oxide nanoparticles, Carbon 80 (2014) 356-363.
[29] B. Dalkıran, P.E. Erden, E. Kılıç, Amperometric biosensors based on carboxylated multiwalled carbon nanotubes-metal oxide nanoparticles-7,7,8,8-tetracyanoquinodimethane composite for the determination of xanthine, Talanta 167 (2017) 286-295.
[30] A.P. Turner, [7] Amperometric biosensors based on mediator-modified electrodes, Methods in enzymology, Elsevier1988, pp. 90-103.

[31] W. Schuhmann, T.J. Ohara, H.L. Schmidt, A. Heller, Electron transfer between glucose oxidase and electrodes via redox mediators bound with flexible chains to the enzyme surface, J. Am. Chem. Soc. 113(4) (1991) 1394-1397.
[32] A. Chaubey, B. Malhotra, Mediated biosensors, Biosens. Bioelectron. 17(6-7) (2002) 441-456.
[33] H. Deng, A.K.L. Teo, Z. Gao, An interference-free glucose biosensor based on a novel low potential redox polymer mediator, Sens. Actuator B-Chem.191 (2014) 522-528.
[34] Y.-L. Yao, K.-K. Shiu, Low potential detection of glucose at carbon nanotube modified glassy carbon electrode with electropolymerized poly (toluidine blue O) film, Electrochim. Acta 53(2) (2007) 278-284.
[35] G.-M. Zeng, L. Tang, G.-L. Shen, G.-H. Huang, C.-G. Niu, Determination of trace chromium (VI) by an inhibition-based enzyme biosensor incorporating an electropolymerized aniline membrane and ferrocene as electron transfer mediator, Int. J. Environ. An Ch. 84(10) (2004) 761-774.
[36] A. Attar, M.E. Ghica, A. Amine, C.M. Brett, Poly (neutral red) based hydrogen peroxide biosensor for chromium determination by inhibition measurements, , J. Hazard. Mater. 279 (2014) 348-355.
[37] J. Li, Y. Yu, J. Qian, Y. Wang, J. Zhang, J. Zhi, A novel integrated biosensor based on co-immobilizing the mediator and microorganism for water biotoxicity assay, Analyst 139(11) (2014) 2806-2812.
[38] N. Morris, M. Cardosi, B. Birch, A. Turner, An electrochemical capillary fill device for the analysis of glucose incorporating glucose oxidase and ruthenium (III) hexamine as mediator, Electroanal. 4(1) (1992) 1-9.
[39] A.D. Ryabov, V.S. Sukharev, L. Alexandrova, R. Le Lagadec, M. Pfeffer, New synthesis and new bio-application of cyclometalated ruthenium (II) complexes for fast mediated electron transfer with peroxidase and glucose oxidase, Inorg. Chem. 40(25) (2001) 6529-6532.
[40] W. da Silva, M.E. Ghica, C.M. Brett, Biotoxic trace metal ion detection by enzymatic inhibition of a glucose biosensor based on a poly (brilliant green)–deep eutectic solvent/carbon nanotube modified electrode, Talanta 208 (2020) 120427.
[41] W. da Silva, M.E. Ghica, C.M. Brett, Choline oxidase inhibition biosensor based on poly (brilliant cresyl blue)–deep eutectic solvent/carbon nanotube modified electrode for dichlorvos organophosphorus pesticide, Sens. Actuator B Chem. 298 (2019) 126862.
[42] P.N. Nomngongo, J.C. Ngila, V.O. Nyamori, E.A. Songa, E.I. Iwuoha, Determination of selected heavy metals using amperometric horseradish peroxidase (HRP) inhibition biosensor, Anal. Let. 44(11) (2011) 2031-2046.
[43] M.E. Ghica, C.M. Brett, Glucose oxidase inhibition in poly (neutral red) mediated enzyme biosensors for heavy metal determination, Microchim. Acta 163(3-4) (2008) 185-193.
[44] A. Berezhetskyy, O. Sosovska, C. Durrieu, J.-M. Chovelon, S. Dzyadevych, C. Tran-Minh, Alkaline phosphatase conductometric biosensor for heavy-metal ions determination, Irbm 29(2-3) (2008) 136-140.
[45] T. Ibrahim, E. Erhan, P. KARAGOeZ, M. OeZKAN, Determination of mercury and nickel by amperometric biosensor prepared with thermostable lactate dehydrogenase, T. Nonferr. Metal Soc. 21(10) (2011) 2332-2338.
[46] Fallahzadeh, R. A., Ghaneian, M. T., Miri, M., & Dashti, M. M. (2017). Spatial analysis and health risk assessment of heavy metals concentration in drinking water resources. Environmental Science and Pollution Research, 24(32), 24790-24802.
[47] F. Deyhimi, M. Bajalan, Urea enzymatic hydrolysis reaction: Optimization by response surface methodology based on potentiometric measurements, Bioelectrochem. 74(1) (2008) 176-182.

[48] M.R. Guascito, C. Malitesta, E. Mazzotta, A. Turco, Inhibitive determination of metal ions by an amperometric glucose oxidase biosensor: Study of the effect of hydrogen peroxide decomposition, Sens. Actuator B Chem. 131(2) (2008) 394-402.
[49] E. Katz, I. Willner, Probing biomolecular interactions at conductive and semiconductive surfaces by impedance spectroscopy: routes to impedimetric immunosensors, DNA-sensors, and enzyme biosensors, Electroanalysis: An International Journal Devoted to Fundamental and Practical Aspects of Electroanal. 15(11) (2003) 913-947.
[50] V. Suryanarayanan, S. Yoshihara, T. Shirakashi, Electrochemical behavior of carbon electrodes in organic liquid electrolytes containing tetrafluoroborate and hexafluorophosphate anionic species in different non-aqueous solvent systems, Electrochim. acta 51(5) (2005) 991-999.
[51] C. Erdem, D.K. Zeybek, G. Aydoğdu, B. Zeybek, Ş. Pekyardımcı, E. Kılıç, Electrochemical glucose biosensor based on nickel oxide nanoparticle-modified carbon paste electrode, Artif. Cell. Nanomed. B. 42(4) (2014) 237-244.
[52] M.M. Barsan, E.M. Pinto, C.M. Brett, Electrosynthesis and electrochemical characterisation of phenazine polymers for application in biosensors, Electrochim. Acta 53(11) (2008) 3973-3982.
[53] S.Z. Mousavisani, J.B. Raoof, R. Ojani, Z. Bagheryan, An impedimetric biosensor for DNA damage detection and study of the protective effect of deferoxamine against DNA damage, Bioelectrochem. 122 (2018) 142-148.
[54] V. Ganesh, S.K. Pal, S. Kumar, V. Lakshminarayanan, Self-assembled monolayers (SAMs) of alkoxycyanobiphenyl thiols on gold—A study of electron transfer reaction using cyclic voltammetry and electrochemical impedance spectroscopy, J. Colloid Interface Sci. 296(1) (2006) 195-203.
[55] D.S. Özdemir, C. Kaçar, B. Dalkıran, S. Küçükkolbaşı, P.E. Erden, E. Kılıç, Effect of hexaammineruthenium chloride and/or horseradish peroxidase on the performance of hydrogen peroxide (bio) sensors: a comparative study, J. Mater. Sci. 54(7) (2019) 5381-5398.
[56] Y. Astier, G.W. Canters, J.J. Davis, H.A.O. Hill, M.P. Verbeet, H.J. Wijma, Sensing nitrite through a pseudoazurin–nitrite reductase electron transfer relay, ChemPhysChem. 6(6) (2005) 1114-1120.
[57] J.C. Vidal, M.A. Yague, J.R. Castillo. A chronoamperometric sensor for hydrogen peroxide based on electron transfer between immobilized horseradish peroxidase on a glassy carbon electrode and a diffusing ferrocene mediator. Sens. Actuator B Chem. 21 (1994) 135-14.
[58] F. Trudeau, F. Daigle, D. Leech, Reagentless mediated laccase electrode for the detection of enzyme modulators, Anal. Chem. 69(5) (1997) 882-886.
[59] W. Li, Z. Wang, C. Sun, M. Xian, M. Zhao, Fabrication of multilayer films containing horseradish peroxidase and polycation-bearing Os complex by means of electrostatic layer-by-layer adsorption and its application as a hydrogen peroxide sensor, Anal. Chimica Acta 418(2) (2000) 225-232.
[60] C. Ren, Y. Song, Z. Li, G. Zhu, Hydrogen peroxide sensor based on horseradish peroxidase immobilized on a silver nanoparticles/cysteamine/gold electrode, Anal. Bio. Chem. 381(6) (2005) 1179-1185.
[61] G.-S. Lai, H.-L. Zhang, D.-Y. Han, Amperometric hydrogen peroxide biosensor based on the immobilization of horseradish peroxidase by carbon-coated iron nanoparticles in combination with chitosan and cross-linking of glutaraldehyde, Microchim. Acta 165 (1-2) (2009) 159-165.
[62] D. Shan, Q.-B. Li, S.-N. Ding, J.-Q. Xu, S. Cosnier, H.-G. Xue, Reagentless biosensor for hydrogen peroxide based on self-assembled films of horseradish peroxidase/laponite/chitosan

and the primary investigation on the inhibitory effect by sulfide, Biosens. Bioelectron. 26(2) (2010) 536-541.
[63] Y. Han, J. Zheng, S. Dong, A novel nonenzymatic hydrogen peroxide sensor based on Ag–MnO2–MWCNTs nanocomposites, Electrochimica Acta 90 (2013) 35-43.
[64] C.R.T. Tarley, G. Silveira, W.N.L. dos Santos, G.D. Matos, E.G.P. da Silva, M.A. Bezerra, M. Miró, S.L.C. Ferreira, Chemometric tools in electroanalytical chemistry: methods for optimization based on factorial design and response surface methodology, Microchem. Journal 92(1) (2009) 58-67.
[65] İ.O. Koçoğlu, P.E. Erden, A. Kenar, E. Kılıç, Application of central composite design for the optimization of electrode surface composition for glucose biosensor fabrication, Anal. Bio. Chem. 411(2) (2019) 413-425.
[66] C.V. Uliana, J.O. Tognolli, H. Yamanaka, Application of factorial design experiments to the development of a disposable amperometric DNA biosensor, Electroanal. 23(11) (2011) 2607-2615.
[67] Y. Yang, M. Yang, H. Wang, J. Jiang, G. Shen, R. Yu, An amperometric horseradish peroxidase inhibition biosensor based on a cysteamine self-assembled monolayer for the determination of sulfides, Sens. Actuator B-Chem.102(1) (2004) 162-168.
[68] N.H. Al-Hardan, A. Hamid, M. Azmi, R. Shamsudin, N.K. Othman, L. Kar Keng. Amperometric non-enzymatic hydrogen peroxide sensor based on aligned zinc oxide nanorods. Sensors 16(7) (2016) 1004.
[69] E. Koposova, X. Liu, A. Kisner, Y. Ermolenko, G. Shumilova, A. Offenhäusser, Y. Mourzina. Bioelectrochemical systems with oleylamine-stabilized gold nanostructures and horseradish peroxidase for hydrogen peroxide sensor, Biosens. Bioelectron. 57, (2014) 54-58.
[70] J. Yuan, S. Xu, H.Y. Zeng, X. Cao, A.D. Pan, G.F. Xiao, P.X. Ding. Hydrogen peroxide biosensor based on chitosan/2D layered double hydroxide composite for the determination of H_2O_2. Bioelectrochem. 123 (2018) 94-102.
[71] W. Liu, Z. Zhou, L. Yin, Y. Zhu, J. Zhao, B. Zhu, L. Wang. A novel self-powered bioelectrochemical sensor based on $CoMn_2O_4$ nanoparticle modified cathode for sensitive and rapid detection of hydrogen peroxide. Sens. Actuators B Chem. 271 (2018) 247-255.
[72] F.N. Kok, F. Bozoglu, V. Hasirci, Construction of an acetylcholinesterase–choline oxidase biosensor for aldicarb determination, Biosens. Bioelectron. 17(6-7) (2002) 531-539.
[73] B. Dalkıran, P.E. Erden, E. Kılıç, Graphene and tricobalt tetraoxide nanoparticles based biosensor for electrochemical glutamate sensing, Artif. Cell. Nanomed. B. 45(2) (2017) 340-348.
[74] C. Chen, X. Hong, T. Xu, A. Chen, L. Lu, Y. Gao, Hydrogen peroxide biosensor based on the immobilization of horseradish peroxidase onto a poly (aniline-co-N-methylthionine) film, Synth. Met. 212 (2016) 123-130.
[75] J. Yuan, S. Xu, H.-Y. Zeng, X. Cao, A.D. Pan, G.-F. Xiao, P.-X. Ding, Hydrogen peroxide biosensor based on chitosan/2D layered double hydroxide composite for the determination of H_2O_2, Bioelectrochem. 123 (2018) 94-102.
[76] K.A. Joshi, J. Tang, R. Haddon, J. Wang, W. Chen, A. Mulchandani, A disposable biosensor for organophosphorus nerve agents based on carbon nanotubes modified thick film strip electrode, Electroanal. 17(1) (2005) 54-58.
[77] E. Forgiarini, A.A.U. de Souza, Toxicity of textile dyes and their degradation by the enzyme horseradish peroxidase (HRP), , J. Hazard. Mater. 147(3) (2007) 1073-1078.
[78] F. Kuralay, H. Özyörük, A. Yıldız, Inhibitive determination of Hg2+ ion by an amperometric urea biosensor using poly (vinylferrocenium) film, Enzyme Microb. Technol. 40(5) (2007) 1156-1159.
[79] M. Moyo, J.O. Okonkwo, N.M. Agyei, An amperometric biosensor based on horseradish peroxidase immobilized onto maize tassel-multi-walled carbon nanotubes modified glassy

carbon electrode for determination of heavy metal ions in aqueous solution, Enzyme Microb. Technol. 56 (2014) 28-34.
[80] L. Liu, Z. Chen, S. Yang, X. Jin, X. Lin, A novel inhibition biosensor constructed by layer-by-layer technique based on biospecific affinity for the determination of sulfide, Sens. Actuator B Chem. 129(1) (2008) 218-224.
[81] M. Dixon, The determination of enzyme inhibitor constants, Biochem. J. 55(1) (1953) 170.
[82] A. Cornish-Bowden, A simple graphical method for determining the inhibition constants of mixed, uncompetitive and non-competitive inhibitors, Biochem. J. 137(1) (1974) 143-144.
[83] M. Santimone, R. Koukiekolo, Y. Moreau, V. Le Berre, P. Rougé, G. Marchis-Mouren, V. Desseaux, Porcine pancreatic α-amylase inhibition by the kidney bean (Phaseolus vulgaris) inhibitor (α-AI1) and structural changes in the α-amylase inhibitor complex, BBA Proteins Proteom. 1696(2) (2004) 181-190.
[84] M. Eguilaz, L. Agüí, P. Yanez-Sedeno, J.M. Pingarron. A biosensor based on cytochrome c immobilization on a poly-3-methylthiophene/multi-walled carbon nanotubes hybrid-modified electrode. Application to the electrochemical determination of nitrite, J. Electroanal.Chem. 644(1) (2010) 30-35.
[85] B. Serra, M.D Morales, A.J. Reviejo, E.H. Hall, J.M. Pingarron. Rapid and highly sensitive electrochemical determination of alkaline phosphatase using a composite tyrosinase biosensor. Anal. Biochem. 336(2) (2005) 289-294.
[86] M.E. Ghica, R.C. Carvalho, A. Amine, C.M. Brett, Glucose oxidase enzyme inhibition sensors for heavy metals at carbon film electrodes modified with cobalt or copper hexacyanoferrate, Sens. Actuator B Chem. 178 (2013) 270-278.
[87] J.G. Ayenimo, S.B. Adeloju, Rapid amperometric detection of trace metals by inhibition of an ultrathin polypyrrole-based glucose biosensor, Talanta 148 (2016) 502-510.
[88] M.B. Gumpu, M. Veerapandian, U.M. Krishnan, J.B.B. Rayappan, Amperometric determination of As (III) and Cd (II) using a platinum electrode modified with acetylcholinesterase, ruthenium (II)-tris (bipyridine) and graphene oxide, Microchim. Acta 185(6) (2018) 297.
[89] I. Lapėnaitė, B. Kurtinaitienė, L. Pliuškys, V. Laurinavičius, I. Bachmatova, L. Marcinkevičienė, A. Ramanavičius, Application of PQQ-GDH based polymeric layers in design of biosensors for detection of heavy metals, Mater. Sci. 9(4) (2003) 431-435.
[90] B.B. Rodriguez, J.A. Bolbot, I.E. Tothill, Development of urease and glutamic dehydrogenase amperometric assay for heavy metals screening in polluted samples, Biosens. Bioelectron. 19(10) (2004) 1157-1167.
[91] D. Bagal-Kestwal, M.S. Karve, B. Kakade, V.K. Pillai, Invertase inhibition based electrochemical sensor for the detection of heavy metal ions in aqueous system: Application of ultra-microelectrode to enhance sucrose biosensor's sensitivity, Biosens. Bioelectron. 24(4) (2008) 657-664.
[92] P. Pal, D. Bhattacharyay, A. Mukhopadhyay, P. Sarkar, The detection of mercury, cadium, and arsenic by the deactivation of urease on rhodinized carbon, Environ. Eng. Sci. 26(1) (2009) 25-32.
[93] M.J. Varjovi, R.E. Sabzi, S.M. Borghei, Determination of heavy metal ions by an amperometric biosensor based on glucose oxidase immobilized onto single-walled carbon nanotubes/Nile blue nanocomposite. J. Iran. Chem. Soc. 15(8) (2018) 1765-1774.
[94] A.Q. Mugheri, A. Tahira, S.T.H. Sherazi, M.I. Abro, M. Willander, Z.H. Ibupoto, An amperometric indirect determination of heavy metal ions through inhibition of glucose oxidase immobilized on cobalt oxide nanostructures. Sensor Lett. 14(12) (2016) 1178-1186.
[95] H.S. Magar, M.E. Ghica, M.N. Abbas, C.M. Brett, Highly sensitive choline oxidase enzyme inhibition biosensor for lead ions based on multiwalled carbon nanotube modified glassy carbon electrodes. Electroanal. 29(7) (2017) 1741-1748.

Declaration of interests

☒ The authors declare that they have no known competing financial interests or personal relationships that could have appeared to influence the work reported in this paper.

☐The authors declare the following financial interests/personal relationships which may be considered as potential competing interests:

Highlights

- A novel HRP inhibition biosensor based on ITO, RUT and CH were fabricated
- The amounts of ITO and RUT were optimized using a central composite design
- Heavy metals were successfully determined in sample with nanomolar detection limits
- The results obtained from the presented method had good agreement with AAS results